Received: 3 June 2019 | Revised: 6 April 2020 | Accepted: 26 April 2020

DOI: 10.1002/hbm.25035

RESEARCH ARTICLE

WILEY

EEG source-space synchrostate transitions and Markov modeling in the math-gifted brain during a long-chain reasoning task

Li Zhang[1] | John Q. Gan[2] | Yanmei Zhu[3] | Jing Wang[4] | Haixian Wang[3]

[1]School of Medical Imaging, Bengbu Medical College, Bengbu, Anhui, China

[2]School of Computer Science and Electronic Engineering, University of Essex, Colchester, UK

[3]Key Laboratory of Child Development and Learning Science of Ministry of Education, School of Biological Science and Medical Engineering, Southeast University, Nanjing, Jiangsu, China

[4]School of Computer Science and Information Technology, Xinyang Normal University, Xinyang, Henan, China

Correspondence
Haixian Wang, School of Biological Science and Medical Engineering, Southeast University, 2 Sipailou Road, Nanjing, Jiangsu 210096, China.
Email: hxwang@seu.edu.cn

Funding information
China Scholarship Council Fund, Grant/Award Number: 201808340011; Fundamental Research Funds for the Central Universities, Grant/Award Number: CDLS-2018-04; National Natural Science Foundation of China, Grant/Award Numbers: 31600862, 31900710, 61773114; Scientific Research Innovation Project of Bengbu Medical College, Grant/Award Number: BYKC201905; Support Program of Excellent Young Talents in Universities of Anhui Province, Grant/Award Number: gxyqZD2017064

Abstract

To reveal transition dynamics of global neuronal networks of math-gifted adolescents in handling long-chain reasoning, this study explores momentary phase-synchronized patterns, that is, electroencephalogram (EEG) synchrostates, of intracerebral sources sustained in successive 50 ms time windows during a reasoning task and non-task idle process. Through agglomerative hierarchical clustering for functional connectivity graphs and nested iterative cosine similarity tests, this study identifies seven general and one reasoning-specific prototypical functional connectivity patterns from all synchrostates. Markov modeling is performed for the time-sequential synchrostates of each trial to characterize the interstate transitions. The analysis reveals that default mode network, central executive network (CEN), dorsal attention network, cingulo-opercular network, left/right ventral frontoparietal network, and ventral visual network aperiodically recur over non-task or reasoning process, exhibiting high predictability in interactively reachable transitions. Compared to non-gifted subjects, math-gifted adolescents show higher fractional occupancy and mean duration in CEN and reasoning-triggered transient right frontotemporal network (rFTN) in the time course of the reasoning process. Statistical modeling of Markov chains reveals that there are more self-loops in CEN and rFTN of the math-gifted brain, suggesting robust state durability in temporally maintaining the topological structures. Besides, math-gifted subjects show higher probabilities in switching from the other types of synchrostates to CEN and rFTN, which represents more adaptive reconfiguration of connectivity pattern in the large-scale cortical network for focused task-related information processing, which underlies superior executive functions in controlling goal-directed persistence and high predictability of implementing imagination and creative thinking during long-chain reasoning.

KEYWORDS

agglomerative hierarchical clustering, EEG source-space synchrostate, logical reasoning, Markov chain modeling, math-gifted adolescents

1 | INTRODUCTION

In the field of educational neuroscience, math-gifted adolescents/children have been drawing much attention on their "atypical" brain and "atypical" brain functioning (Winner, 2000), which account for above-normal intelligence and specific talent in mathematics, especially exceptional traits in solving long-chain reasoning problems (Banfield, 2005). Previous neuroimaging studies have revealed the major neural characteristics of math-gifted brain in both structure and functioning, primarily including superior cognitive controlling functions of the prefrontal cortex (PFC), highly developed right hemisphere and heightened interhemispheric interaction via the corpus callosum, enhanced frontal connectivity between the dorsolateral prefrontal cortex (DLPFC) and premotor cortex, and strengthened anterior–posterior interaction in the frontoparietal network during reasoning, visuospatial imagery or creative thinking tasks (Desco et al., 2011; Myers, Carey, & Szűcs, 2017; Navas-Sánchez et al., 2014, 2016; Prescott, Gavrilescu, Cunnington, O'Boyle, & Egan, 2010; Zhang, Gan, & Wang, 2017). Importantly, the well-developed frontoparietal network, especially increased anatomical connectivity in frontoparietal association tracts, has been suggested as a crucial neural correlate of specific giftedness in mathematics independent of subjects' high-level intelligence scores (Navas-Sánchez et al., 2014).

Because of the crucial role in mathematical thinking and problem-solving, the frontal–parietal network of the math-gifted brain is worth more in-depth data mining research. Recent findings from dynamic functional connectivity (DFC) have provided new insight into rapid fluctuations in the brain network structure underlying discrete epoch of ongoing cognitive function (Duc & Lee, 2019; Mahyari, Zoltowski, Bernat, & Aviyente, 2016). Through tracking dynamic interaction among brain regions during the execution of a task, DFC analysis of brain network can facilitate a better understanding of sub-second brain dynamics involved in sensation, perception, high-order cognition, emotion, mental disorders, and so forth (Dimitriadis, Laskaris, & Micheloyannis, 2015; Dimitriadis, Laskaris, & Tzelepi, 2013; Dimitriadis, López, Maestu, & Pereda, 2019; Karamzadeh, Medvedev, Azari, Gandjbakhche, & Najafizadeh, 2013; Michel & Koenig, 2017). Being related to the criticality of phase synchrony, metastable interactions or connections within a functional network can flexibly adapt and continuously evolve from one coordination system to another, which is supposed to be the neurophysiological basis for cognitive and behavioral adaption (Allen et al., 2014; Bassett et al., 2011; Bola & Sabel, 2015; Kitzbichler, Smith, Christensen, & Bullmore, 2009). By investigating frequency-specific phase synchronizations in the multichannel electroencephalogram (EEG) or magnetoencephalogram signals, some studies have revealed that there are a limited number of quasi-stable connectivity patterns in functional brain networks (about 100–200 ms), named synchrostates or functional connectivity microstates (Baker et al., 2014; Daly, Sweeney-Reed, & Nasuto, 2013; Dimitriadis et al., 2013; Dimitriadis et al., 2015; Jamal, Das, & Maharatna, 2013; Jamal, Das, Oprescu, & Maharatna, 2014). Specifically, these synchrostates undergo interstate transitions following a well-defined Markov chain, showing distinctive probabilistic transition modes in different cognitive tasks or different groups of populations (Baker et al., 2014; Jamal et al., 2015; Rothmaler & Ivanova, 2018; Rukat, Baker, Quinn, & Woolrich, 2016).

During the problem-solving process, an exceptional logical capability is the major characteristic of math-gifted adolescents, especially the ability to handle long chains of deductive reasoning (Banfield, 2005). The previous studies on math-gifted adolescents made use of related measurements from time average or time interval covering the whole cognitive task period, regardless of the fact that high-level cognition, such as logical reasoning, usually contains multiple heterogeneous cognitive subprocesses and information processing stages (Yule, Fox, Glasspool, & Cooper, 2013). From the perspective of brain microstates, a complex cognitive process is constructed by a series of focused and momentarily assembled temporal fragments, and thus brain activity can be divided into a chain of transient and quasi-stable spatiotemporal activity patterns (Duncan, 2013; Michel & Koenig, 2017). In some DFC studies, math-gifted adolescents showed highly adaptive functional network reorganization in both high- and low-frequency neuronal oscillations while coping with varying cognitive requirements (Zhang, Gan, & Wang, 2014, 2015). Besides, a structural brain network study has demonstrated that gifted children have more integrated and versatile topology (Solé-Casals et al., 2019). Therefore, further time-frequency decomposition of functional networks and statistical modeling for the pseudorandom switching relationship among discrete synchrostates could establish spatiotemporal patterns of the interstate transition of ongoing brain activity, which might imply specific rules of the adaptive reorganization of large-scale neuronal networks related to high-level ability in the persistent problem-solving process.

Unlike previous sensor-level analysis of EEG synchrostates, this study extends brain signals to reconstructed cortical sources, for reducing volume conduction effect on functional network analysis and better estimating the synchronized activities among intracerebral cortical regions. On the basis of a single-trial analysis of phase-synchronized networks for both math-gifted and non-gifted subjects, time-sequential synchrostates are constructed in consecutive 50 ms time windows along a 9,000 ms three-stage deductive reasoning task and a time-matched task-free process. With the consideration of individual variability in brain network topology, the agglomerative hierarchical clustering (AHC) method is adopted to cluster an individual's functional connectivity graphs (FCGs). Through further integrating subject-specific clusters, this study extracts a limited number of general functional connectivity patterns as the prototypical networks. After that, nested iterative cosine similarity tests are conducted to reallocate every synchrostate back to its "optimal" cluster(class) and update the prototypes, until the prototypical connectivity patterns become stabilized. From interstate transition probability matrices, this study establishes and statistically compares the Markov chains of synchrostate sequences formed in different task conditions and subject groups, so as to further distinguish and discuss the probabilistic transition patterns specific to the logical thinking process of the math-gifted brain.

2 | MATERIALS AND METHODS

2.1 | EEG experiment and data acquisition

2.1.1 | Participants

In this study, the math-gifted group was composed of 12 subjects including nine males and three females aged 16.5 ± 0.7 (mean ± *SD*), who were selected from the Science and Engineering Experimental Class at Southeast University, Nanjing, China. Three basic criteria were carried out to screen the math-gifted subjects, that is, teachers' nomination and evaluation on math talent from performance-based observation, award-winning experience in at least one of some important mathematical competitions (e.g., Maths Olympic Competition), and intelligence test scores on Raven's Advanced Progressive Matrices (RAPM) (higher than 32). The control group consisted of 14 subjects including eight males and six females aged 15.4 ± 0.4 (mean ± *SD*), who were from the Fourth Nanjing High School and had average-level mathematical performance in school tests and intelligence scores in RAPM tests. The exclusion criteria for all subjects included left-handedness, medical, neurological, or psychiatric illness, and history of brain injury or surgery.

The experiment was approved by the Academic Committee of the Research Center for Learning Science, Southeast University, China. Before the experiment, all subjects and their guardians were informed of the detailed experimental requirements and signed a fully informed consent form. After accomplishing the experimental task, the subjects received financial compensation for their participation.

2.1.2 | Experimental task

As a standard type of deductive reasoning, a categorical syllogism task of verbal-logical type was performed by all the subjects. The task consists of three successive stages, that is, a major premise, a minor premise, and a conclusion. The major and minor premises are composed of abstract letter items, from which the subjects were asked to infer the relationship implied between the given items and make a judgment in the conclusion stage. Neuroimaging studies have identified that the complex of multiple brain regions, including frontal, parietal, temporal, and occipital regions, is involved in the categorical syllogism reasoning process (Goel & Dolan, 2001).

In this experiment, there are 64 task trials, composed of 32 valid and 32 invalid reasoning problems, and 40 non-task baseline trials. For the reasoning task, each valid trial contains syllogistic sentences following true logical rules, but in an invalid trial, the relationship among three syllogistic sentences is illogical, inconclusive, or incorrect. Besides, the non-task baseline trials consist of the same letter items in each sentence, in order to just match the time course of the valid and invalid reasoning trials.

As illustrated in Figure 1, the stimuli for each trial were presented along the timeline, with the total time length of 9,500 ms. The valid, invalid, and baseline trials were cross-presented with a pseudorandom probability. Following the presentation of symbol "+" for 1,000 ms and a black screen for 500 ms, the major premise, minor premise, and conclusion appeared in order on the screen for 3,000 ms, respectively. After the conclusion of a valid or invalid reasoning trial had been presented, the subjects were asked to judge whether the conclusion was correct or not, by pressing "K" for right and "D" for wrong. When a baseline trial with the same letter items was shown, the subjects just needed to quietly stare at the screen until the end of the entire presentation, without the requirement of conscious thought about the relationship between letter items. Before the formal experiment, a practice procedure containing 15 trials equally allocated for the three types was performed by the subjects. After that, they could decide to quit, practice again, or start the formal procedure. In the middle period of the task course, there was a pause when subjects could decide the time for a short break to avoid mental fatigue. For each subject, the total time length of the experimental task was about 30 min.

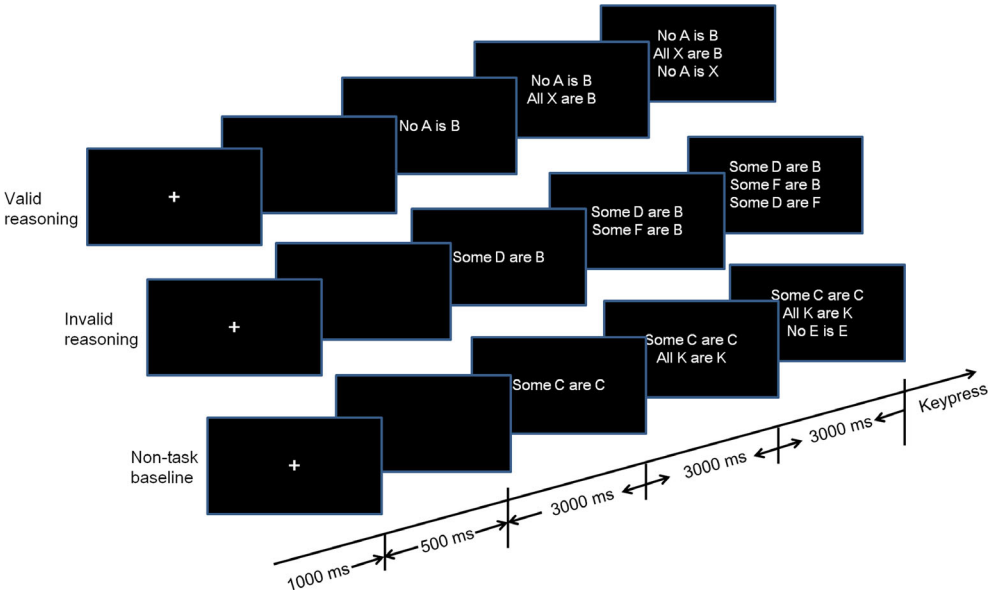

FIGURE 1 Timeline of stimulus presentation of a categorical syllogism task. Top to bottom: examples of a valid reasoning trial, an invalid reasoning trial, and a non-task baseline trial

2.1.3 | Data recording and preprocessing

The EEG data were recorded by the Neuroscan international 10–20 system with 1,000 Hz sampling rate and 60 electrodes covering frontal, parietal, temporal, and occipital regions. Besides, there were two reference electrodes placed on the bilateral mastoids. In order to monitor ocular movements and eye blinks, four surface electrodes were used to simultaneously record electrooculographic (EOG) signals, one pair of which was placed over the higher and lower left eyelids and the other pair was placed 1 cm lateral to the outer corner of the left and right orbits.

The raw EEG data were preprocessed by the Scan 4.3 software. The continuous signals were preliminarily band-pass filtered within a frequency band of 1–100 Hz. Each trial was extracted within a time window of 9,500 ms, with 500 ms for the pre-stimulus time interval and 9,000 ms for the poststimulus period. The baseline correction was performed following the pre-stimulus time interval. According to an EEG-vertical EOG covariance analysis (i.e., a linear regression procedure), ocular artifacts were reduced by performing point-by-point proportional subtraction of the blinks. Besides, the trials contaminated by eye blinks and electrocardiogram noise were excluded through artifact rejection with a threshold of about 50–75 μV. After notch filtering for the removal of 50 Hz line noise, the independent component analysis of the EEGLAB toolbox was run in a trial-by-trial manner, whereby the independent components (ICs) related to visible artifacts were cleared, such as the ICs of ocular and muscle movements (Delorme & Makeig, 2004). As a result, the original EEG data were decomposed into 60 ICs, in which 0–4 ICs were detected and removed for each subject. Finally, 261 reasoning and 234 baseline trials were retained for the math-gifted subjects, and 336 reasoning and 265 baseline trials were available in the non-gifted group, of which 16–35 trials were retained for each subject under each condition.

2.2 | Constructing synchrostate sequences from time-segmented source signals

To establish a sequence of momentarily assembled states of large-scale neuronal oscillatory activity, each trial was parsed into 180 discrete epochs, in which phase-synchronized networks of cortical sources sustained for every 50 ms time windows (i.e., synchrostates) were constructed along the reasoning task course and the task-free baseline process. For accurately detecting state-dependent functional connectivity and its fluctuations that constitute a complete cognitive process, single-trial source data were used in the analysis of phase-locking statistics, with consideration of trial-to-trial variation in brain activities (Lachaux, Rodriguez, Martinerie, & Varela, 1999).

2.2.1 | Cortical source transformation

It has been demonstrated that the source-based construction of phase-synchronized networks could well reduce volume conduction effect on the estimation of authentic functional connectivity of the brain network (Langer et al., 2012; Schmidt, Ghuman, & Huppert, 2014). A source transformation procedure in the Brainstorm toolbox was executed to reconstruct the intracerebral sources of EEG signals in the manner of entire trials (http://neuroimage.usc.edu/brainstorm; Tadel, Baillet, Mosher, Pantazis, & Leahy, 2011). Here, the EEG recording from the scalp sensors was assumed to be composited by a block of electric dipoles at the surface of the cortex of a template MNI brain ("ICBM152" nonlinear atlas). After setting the layers (head, outer skull, and inner skull) and the relative conductivities of each layer, the forward model (i.e., volume conduction modeling for all subjects) was obtained according to a symmetric Boundary Element Model in OpenMEEG software (Gramfort, Papadopoulo, Olivi, & Clerc, 2010). The forward model is also called leadfield matrix (number of sensors × number of sources) related to the activity of the sources to the sensor data. Then, for each individual's trials, the noise of scalp sensors was removed based on the noise covariance matrix of signals in the pre-stimulus interval. The solution to the inverse problem was to estimate the activity of the dipoles described by the forward model. Here, the "illposedness" of the source modeling, that is, using 60 spatial measurements (the number of sensors) as input to estimate the activity of hundreds of dipoles, was dealt with minimum-norm estimation (MNE) by introducing a regularizer or prior in the form of a source covariance that favors minimum energy solutions. By using standardized Low-Resolution brain Electromagnetic Tomography (sLORETA) as the normalization method, the MNE current density map was normalized at each time point. As a result, the sources were mapped to a distributed model composed of 151 dipoles uniformly covering the surface of dorsal and ventral cortices, which were used as the fundamental nodes for the following functional brain network analysis.

2.2.2 | Phase-locking value of γ-band source signals

Phase lock representing synchronization of oscillations is a usual measurement to estimate information integration in the brain, since in phase-locking state the communication windows for input and output between neuronal groups may be open at the same time (Fries, 2005). It is also suggested that a synchronization relationship measured between two neuroelectric signals is derived from true interaction between their corresponding neural sources (Vinck, Oostenveld, Wingerden, Battaglia, & Pennartz, 2011).

After filtering the source signals in a low γ frequency band (30–45 Hz), one of the most relevant frequency bands of cognitive task processing (Duc & Lee, 2019), through linear finite response filter, we computed phase-locking value (PLV) for pairwise time series. Neuronal population oscillating in the γ frequency range can mediate large-scale integration through entering into precise phase-locking activity over a limited period (Lachaux et al., 1999). Besides, γ-band oscillation has also been suggested to be highly involved in various cognitive functions, such as sensation, perception, working memory load, high-order cognition, and so forth. (Herrmann, Fründ, & Lenz, 2010; Howard et al., 2003). Moreover, γ-band phase

synchronization is considered as the important building blocks of the electrical activity of the brain, by undertaking important feature binding function among neuronal populations that underlies a large-scale, transient, and state-dependent functional neurocognitive network (Doesburg, Roggeveen, Kitajo, & Ward, 2008). More importantly, previous dynamic brain network studies have found that the γ-band synchronization network exhibits the highest global synchronizability and temporal lability of topological reorganization in the fractal small-world networks of the human brain (Bassett, Meyer-Lindenberg, Achard, Duke, & Bullmore, 2006).

In the definition of PLV (Lachaux et al., 1999), $x(t)$ and $y(t)$ represent two time series with equal length, and $\varnothing_x(t)$ and $\varnothing_y(t)$ refer to the instantaneous phases of $x(t)$ and $y(t)$, respectively. Phase synchrony indicates the locking of $\varnothing_x(t)$ and $\varnothing_y(t)$ associated with each signal, that is, $|\varnothing_x(t) - \varnothing_y(t)|$ = const. Here, the phase of a signal can be acquired by the Hilbert transform (HT) that constructs an analytical signal $H(t) = x(t) + i\tilde{x}(t)$, where $\tilde{x}(t)$ representing the HT of $x(t)$ is obtained according to $\tilde{x}(t) = \frac{1}{\pi} PV \int_{-\infty}^{\infty} \frac{x(t')}{t-t'} dt'$ (PV is the Cauchy principal value). The phases of $x(t)$ and $y(t)$ are obtained by $\varnothing_x(t) = \arctan\frac{\tilde{x}(t)}{x(t)}$ and $\varnothing_y(t) = \arctan\frac{\tilde{y}(t)}{y(t)}$, respectively. Then, the bivariate metric PLV is produced from

$$PLV = \left| \frac{1}{M} \sum_{j=0}^{M-1} \exp(i(\varnothing_x(\ j\Delta t) - \varnothing_y(\ j\Delta t))) \right| \quad (1)$$

Here, Δt is the sampling period and M refers to the number of sample points of a signal in a specified time window. PLV is always represented by a value between 0 and 1, where 0 signifies purely random rise and fall whereas 1 indicates that one signal perfectly follows the other (Sakkalis, 2011).

In every 50 ms time window, a PLV association matrix was computed for each pair of source signals to produce a functional connectivity network (a synchrostate). Thus, a sequence composed of 180 continuously evolving synchrostates was formed for each trial. By integrating the synchrostates across all time windows and all trials of a subject, under non-task or reasoning condition, this study constructed a set of individual synchrostates with the size equaling (number of trials) × (number of time windows), as shown in Figure 2.

2.2.3 | AHC for individual graphs

For each PLV association matrix of size 151 × 151, an adjacent matrix can be acquired by applying a fixed connection density $p_{den} = 2\ln n/n$ defined by the Erdős-Rényi model (Erdős & Rényi, 1961), where n is the number of nodes. Then, the undirected graphs of synchrostates are obtained from the time-sequential adjacent matrices. From a set of graphs, a limited number of prototypical connectivity patterns, manifested as the repetitive occurrence in temporal sequence, can be reliably identified.

In a binary FCG, let N be the set of all the nodes in a network and (i, j) represent the edge between nodes i and j ($i, j \in N$; $i \neq j$). If there is a connection status between nodes i and j, $A_{ij} = 1$; otherwise, $A_{ij} = 0$ (Bullmore & Sporns, 2009). Based on the connectivity matrix defined

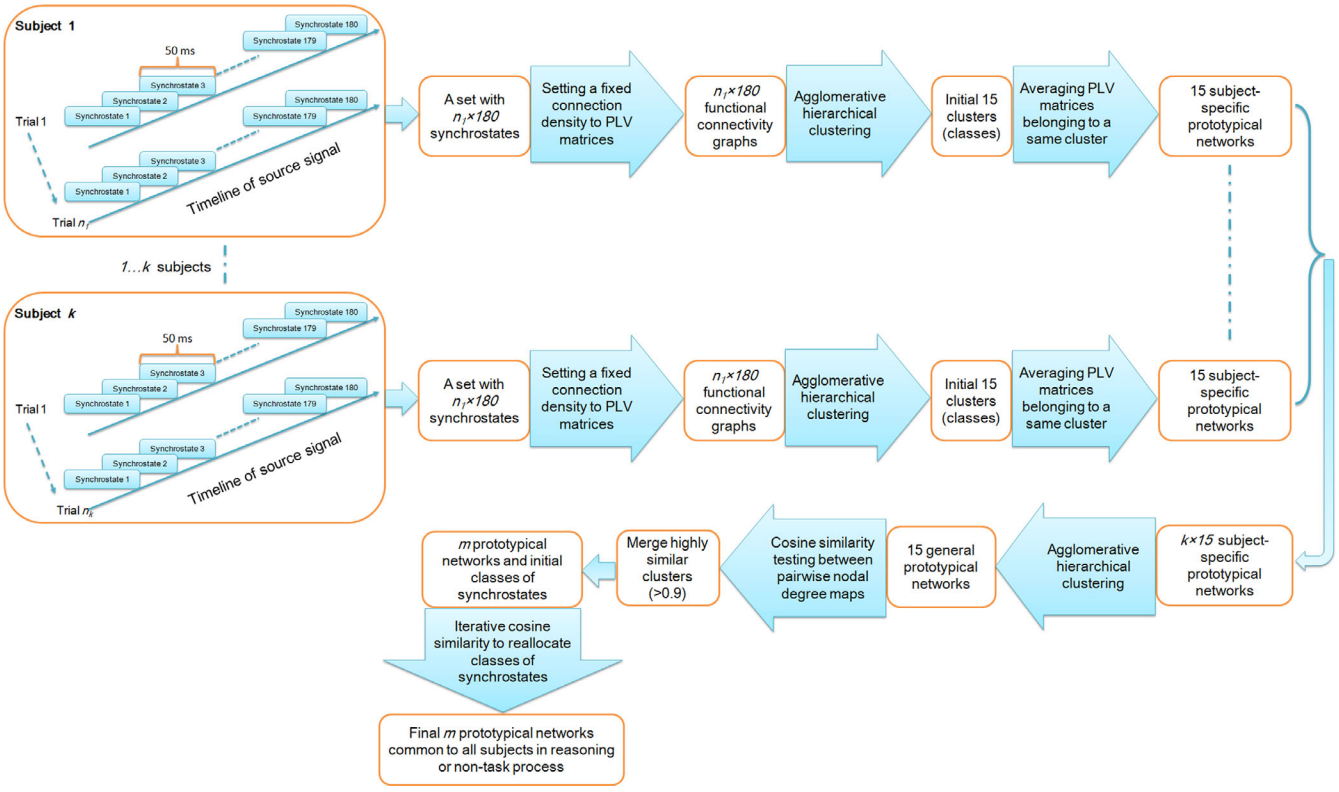

FIGURE 2 Flow diagram of classifying synchrostates and producing prototypical functional networks

by A_{ij}, node degree centrality is equal to the number of connections linked to node i:

$$k_i = \sum_{j \in N} A_{ij} \quad (2)$$

As the most fundamental measure of functional connectivity within a brain connectome, node degree centrality quantifies the structural importance of a node with respect to the rest of the network, especially stronger effects within its own cluster. A node with high degree centrality can be viewed as a provincial hub in a network (Sporns, Honey, & Kötter, 2007; van den Heuvel & Sporns, 2013). Complex brain networks show "heavy-tailed" degree distributions, that is, a small number of nodes having high degree centrality (van den Heuvel & Sporns, 2013). Thus, nodal degree maps were thought to ideally represent local maxima of connection in global neuronal networks.

In the clustering process, we used thresholding FCGs as the topographic features to group these synchrostates. Compared with non-thresholding association matrices, FCGs better represent authentic functional connectivity status, because of the small-world properties of brain networks. Besides, FCG is the binary pattern of the association matrix, where vertices are separated into two disjoint sets. Therefore, FCG is expected to gain better data classification performance in accuracy and speed. As illustrated by the flow diagram in Figure 2, for each set of synchrostates, all synchrostates are represented as a $S \times v$ matrix, where S is the number of observed states and v the feature vectors transformed from FCGs. According to the fixed connection density p_{den} (~0.665) of a 151-node network, the number of connections retained in a FCG is about 753. Using the binary FCGs as the topographic features, the AHC procedure groups these synchrostates into a small number of classes (clusters). Each cluster has a representative connectivity pattern, that is, a prototypical network, which is constructed from the FCG of the averaged association matrix from the synchrostates assigned into the cluster.

Considering individual variability in functional network topology, the clustering procedure was first performed on the basis of an individual's synchrostates. While using a spatial clustering method to identify prototypical topologies of states, the crucial problem is to determine the number of clusters, which is necessary for both capturing the informative features of the data and avoiding over- or under-fitting (Jamal et al., 2013; Michel & Koenig, 2017). Here, the initial number of clusters was set to 15 possible functional connectivity patterns, which were supposed to cover primary large-scale brain networks and cognition-related local subnetworks revealed by previous neuroscience research (Bressler & Menon, 2010). Thus, the AHC procedure grouped the synchrostates for each subject under a condition into 15 clusters, which produced 15 subject-specific prototypical networks. Then, for all subjects, we collected these individual prototypical networks to form a common set, which were then reclassified by the AHC method according to their FCGs. As a result, 15 general prototypes across subjects were obtained. According to the cosine similarity between the nodal degree maps of every two general prototypical networks, the synchrostates from different clusters with high similarity (higher than 0.9) were merged into one larger cluster, and the clusters with too few synchrostates were removed (Figure 2).

2.2.4 | Cosine similarity tests for reallocating synchrostates into optimal clusters

After preliminarily determining the clusters and prototypical network topologies, the classes of synchrostates were iteratively updated by reassigning every synchrostate back to a cluster. As illustrated in the flow diagram of Figure 3, cosine similarity tests were performed between the FCGs of every synchrostate and the prototypical

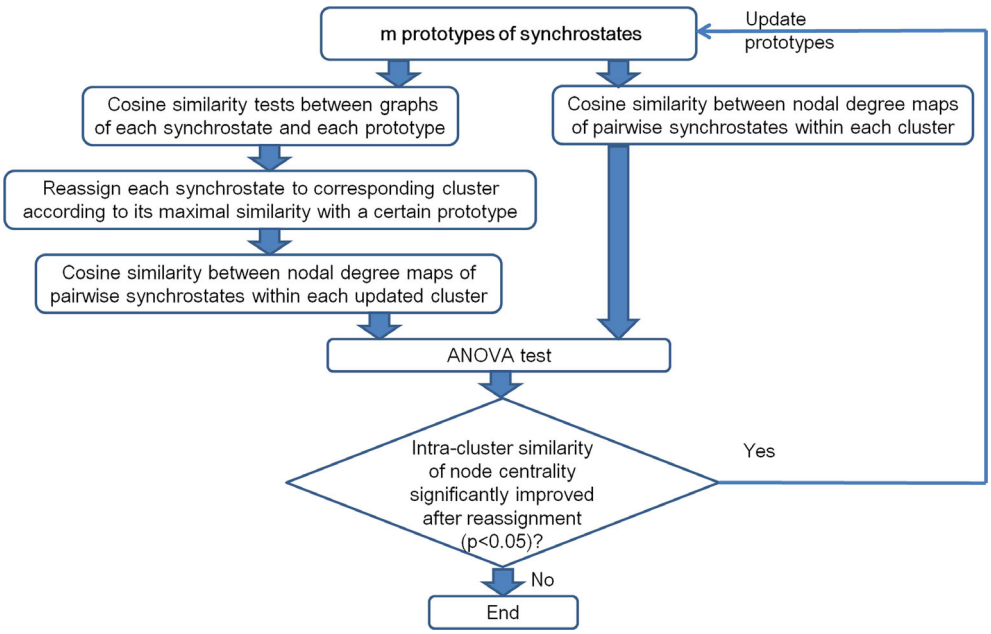

FIGURE 3 Flow diagram of the nested iterative cosine similarity tests for reallocating synchrostates

network of each cluster. According to the maximal cosine similarity with a certain prototype, each synchrostate was reassigned to its corresponding cluster. After that, for the clusters with synchrostates updated, the intra-cluster similarity (i.e., consistency of node centrality) between pairwise nodal degree maps of synchrostates was statistically compared with that of original clusters. If intra-cluster similarity could be significantly improved after the reallocation ($p < .05$ in statistical test), the prototype of the cluster got updated as the result of the mean topology of its reassigned synchrostates. These steps were iteratively executed until there was no further significant improvement of the intra-cluster similarity of node centrality.

After the reallocation procedure, the coefficient of variation (CV) (relative standard deviation) of inter-node PLVs in the functional networks within each cluster was computed to test the topological consistency of the synchrostates labeled with a same class. CV refers to the ratio of the *SD* of data to the mean value, which is a standardized measure characterizing dispersion degree of a distribution. By measuring the extent of variability in relation to the mean of PLVs, CV used here can quantify the variability of internodal phase synchronizations in synchrostates finally assigned into a same cluster.

2.3 | Markov chain modeling for synchrostate transitions

The temporal sequence of mental activity can be described as a Markov process, which predicts the probabilities of a number of discrete states recurring or switching among themselves at different time points (Gärtner, Brodbeck, Laufs, & Schneider, 2015; van de Ville, Britz, & Michel, 2010). Several studies have investigated transition probabilities between phase-synchronized states on a sub-second temporal scale, clearly demonstrating the Markovian property and pseudorandom switching relationship between finite network-level brain states (Baker et al., 2014; Daly et al., 2013; Dimitriadis et al., 2015, 2019).

2.3.1 | Markov process of time-sequential synchrostates

Markov model describes the underlying dynamical nature of a system that follows a chain of linked states, where what happens at any time instant depends only on the preceding one (Gagniuc, 2017). In the Markov chain modeling for synchrostate transitions during the deductive reasoning and the task-free processes, the first-order transition matrices were estimated in a probabilistic framework. According to discrete-time Markov chain theory (Jarvis & Shier, 1999), a finite number (m) of inferred states, $\{S_1, S_2, \ldots, S_m\}$, that evolve in discrete time with a time-homogeneous transition structure can be mathematically represented by either its m-by-m transition probability matrix P or its directed graph (digraph) D. Here, the inferred states represent the prototypical synchrostates from all clusters. A feasible transition is the one whose occurrence probability is greater than zero. The probability of transition from the node (state) a to node b is defined as

$$p_{ab} = N_{ab} / \left(\sum_b N_{ab} \right), a = 1,2,\ldots,m, b = 1,2,\ldots,m \quad (3)$$

where N_{ab} is the number of transitions from node a to node b. Obviously, the sum of the transition probabilities along each row of the transition matrix p equals one. The complete digraph of a finite-state Markov process has edges with transition probabilities between every node a and every other node b. Here, nodes refer to prototypical synchrostates in the Markov chain. In the digraphs created in this study, if p_{ab} is less than a threshold of 0.1, the edge connecting synchrostates a and b is removed in order to clearly show strongly connected components of a digraph. In addition, the digraphs include self-loops with nonzero probability p_{aa} of transition from synchrostate a back to itself (Häggström, 2002).

2.3.2 | Temporal measurements and statistical tests

For further quantitatively assessing inter-synchrostate transition patterns, relevant temporal measurements were extracted from the Markov chain structures of all single-trial synchrostate sequences, including (a) fractional occupancy (occurrence rate) for each class of synchrostates (i.e., the ratio of the number of distinct synchrostates of a given class to the total 180 time windows of a trial), (b) mean duration (i.e., averaged length of time windows lasted for a given network topology during a trial, and (c) transition probabilities of a given synchrostate to any other functional connectivity states. The three measurements were statistically compared by the analysis of variance (AVOVA) between task conditions and between subject groups. Specifically, transition probabilities were tested by the bootstrapped ANOVAs with 1,000 repeated times of random resampling, for assessing the extent to which the differences identified from the Markov process were robust. A false discovery rate (FDR) correction was executed for multiple hypothesis tests in comparing every entry of the transition probability matrices. Besides, between-subjects behavioral data were tested by the ANOVA. The null hypothesis is that there is no difference between conditions or groups, with a significance level being .05.

3 | RESULTS AND DISCUSSION

3.1 | Behavioral performances

A significant group difference was first found in the RAPM test. The math-gifted group exhibited an exceptional level in the testing score, whereas that of the control group was in a normal range (math-gifted vs. non-gifted: 33.5 ± 0.7 vs. 23.7 ± 4.3; ANOVA: $p < .0001$). While performing the reasoning task, the math-gifted adolescents outperformed the control subjects in terms of average response accuracy (math-gifted vs. non-gifted: 75.32 ± 12.50% vs. 65.20 ± 15.32%) and

reaction time of correct responses (math-gifted vs. non-gifted: 837 ± 525 ms vs. 949 ± 610 ms; ANOVA: p = .0465).

3.2 | Prototypical networks representing synchrostates within different clusters

The time-segmented source signals resulted in 107,460 synchrostates during the reasoning process and 89,820 synchrostates in the non-task idle period. Through the clustering procedure and the iterative similarity tests, these short-time phase-synchronized networks were finally separated into different sets of connectivity patterns. Figure 4 shows the changes of intra-cluster similarity of node centrality of synchrostates, which ended up with the 19th iteration for non-task condition and the 12th iteration in reasoning condition.

3.2.1 | General and specific prototypes of synchrostates

The synchrostates assigned into different clusters can be represented by eight prototypical networks. Particularly, seven prototypes are common to non-task idle state and reasoning process, with hub nodes corresponding to the key cortical regions of several well-known fundamental neurocognitive networks, as shown in Figure 5:(a) Synchrostate A: default mode network (DMN). Its hub nodes are primarily distributed at the posterior cingulate cortex, medial PFC, and angular gyrus, with relatively uniform distribution of degree centrality and intensive long-distance synchronizations between medial PFC and PPC (Figure 5a); (b) Synchrostate B: central executive network (CEN). Its key nodes remarkably gather around the DLPFC of left and right cerebral hemispheres, showing dense connections within the DLPFC and interhemispheric interaction (Figure 5b); (c) Synchrostate C: dorsal attention network (DAN). It comprises functionally connected brain regions including visual motion area, frontal eye fields, superior parietal lobule, intraparietal sulcus, and ventral premotor cortex (Figure 5c). (d) Synchrostate D: cingulo-opercular network (CON). It is also referred to as a "salience" network. The provincial hubs of CON are mainly located at anterior insula (AI)/operculum, dorsal anterior cingulate cortex (dACC), and thalamus, accompanying with strengthened phase synchronization activities among them (Figure 5d); (e) synchrostate E and (f) synchrostate F: left and right ventral frontoparietal network (lVFPN/rVFPN). Regions of the two ventral networks comprise dACC and AI, and extend to left and right temporoparietal junction, respectively (Figure 5e,f); (g) Synchrostate G: ventral visual network (VVN). The ventral visual pathway originates from primary visual cortex V1, goes through visual area V2, then through visual area V4, and to the inferior temporal cortex, which processes visual information input of stimulus (Figure 5g). Additionally, an extra cluster was extracted from the synchrostates in the reasoning process, which is (h) Synchrostate H: right frontotemporal network (rFTN). Its central nodes are located at medial and right PFC, dACC, right precentral gyrus, right inferior frontal gyrus, and right temporal pole, with synchronization activity extending to the parietal cortex (Figure 5h).

Furthermore, Figure 6 presents the sequential cortical current maps over the non-task and reasoning process. At the time points of peaks and major waveforms of event-related potential (ERP) components, the responses of sources exhibit spatial correspondence with the nodal degree distribution of prototypical networks. Provincial hubs in a brain network represent converged points for information integration across many different vertices and systems. The spatial correspondence between prototypes of synchrostates and grand average ERP microstates means that the temporal dynamics of the topology of hubs nodes can be predicted and reflected by general neural activation patterns of oscillation amplitude (power).

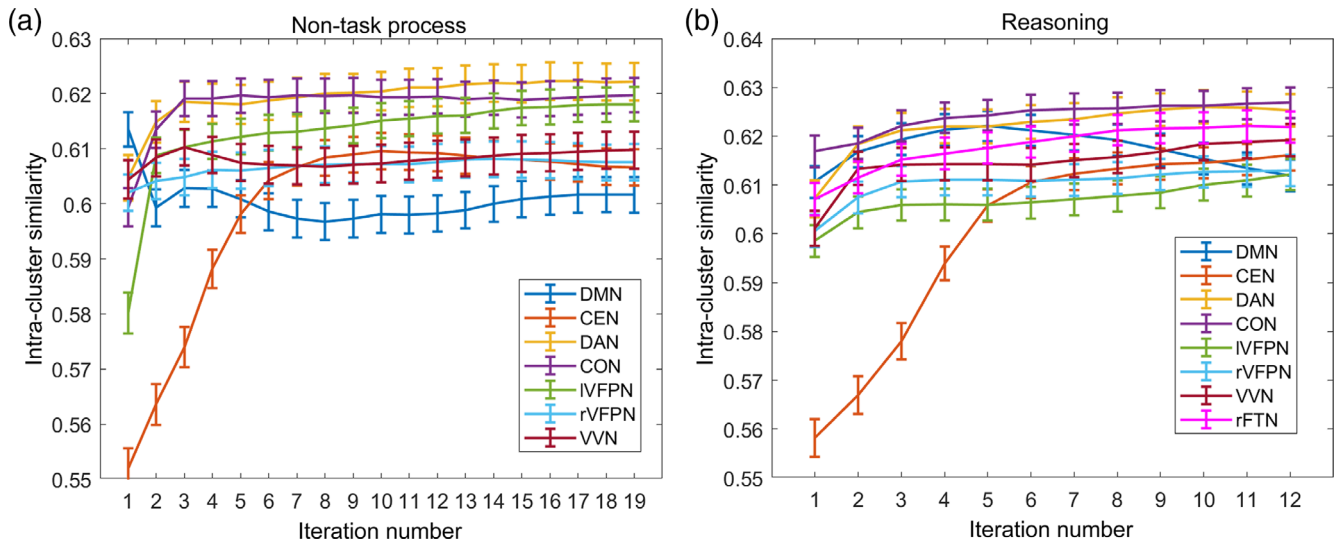

FIGURE 4 Boxplots of intra-cluster similarity of node centrality in iterative tests for each cluster of synchrostates under (a) non-task idle state and (b) reasoning process. The 19th and 12th tests achieved the optimal intra-cluster similarity in the non-task and reasoning process, respectively

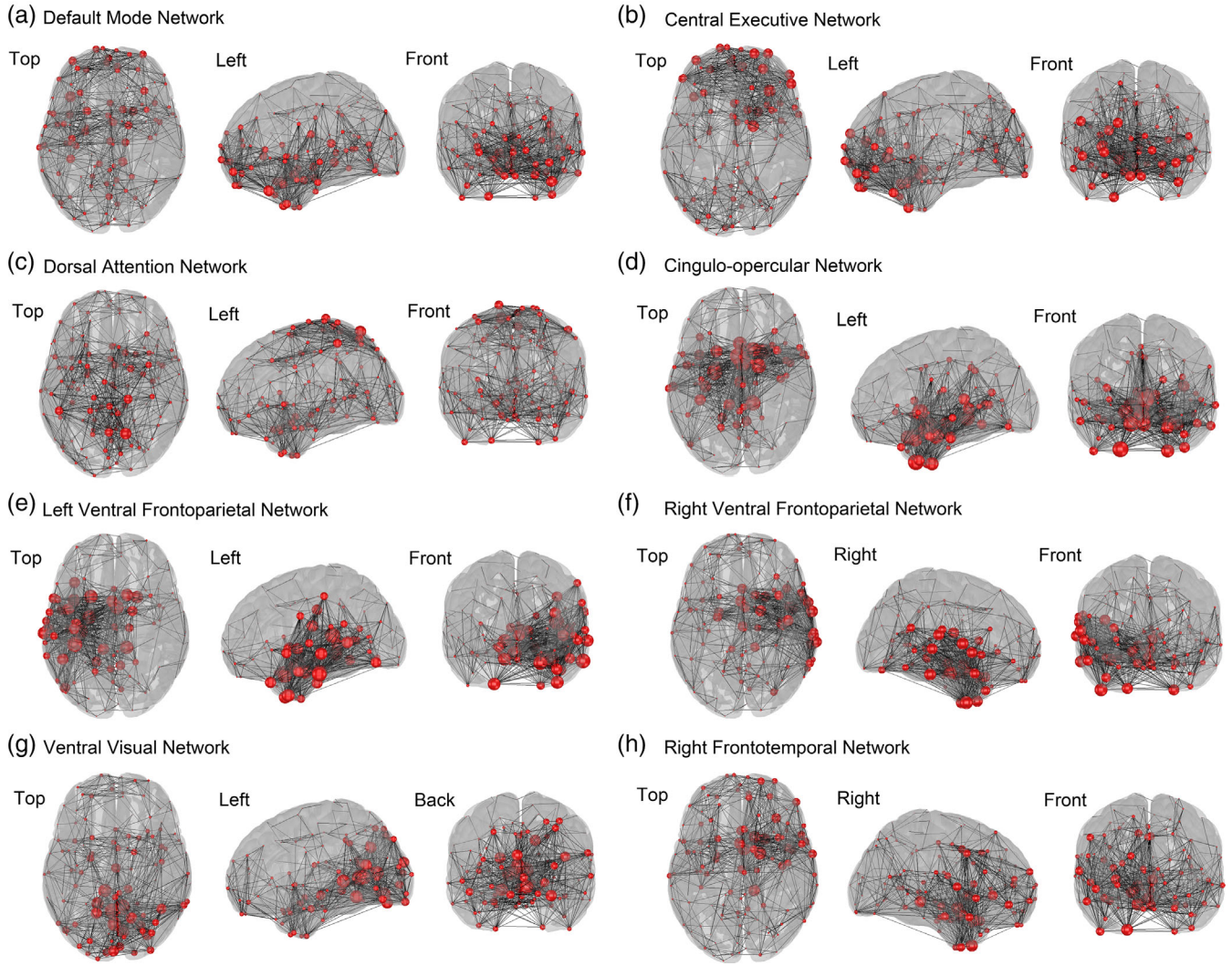

FIGURE 5 Prototypical functional brain networks representing synchrostates within different clusters. During the non-task idle state and reasoning process, the topologies of the prototypical networks correspond to (a) default mode network (DMN), (b) central executive network (CEN), (c) dorsal attention network (DAN), (d) cingulo-opercular network (CON), (e) left ventral frontoparietal network (lVFPN), (f) right ventral frontoparietal network (rVFPN), and (g) ventral visual network (VVN). Besides, an extra (h) right frontotemporal network (rFTN) was formed in the reasoning task course. In a prototypical network, each red ball represents a node, whose diameter is directly proportional to the nodal degree

3.2.2 | Topological similarity of intra-cluster synchrostates

For each cluster, the prototypical network was actually constructed from the averaged PLV matrices of all intra-cluster synchrostates. By this way, inter-synchrostates variations in phase synchronizations among brain areas are weakened but relatively consistent interconnections across synchrostates can get strengthened. The CVs of internodal phase synchronizations were mapped into the source space, in which the synchronized activities with less variability (<0.4) were represented by the links in a topological structure, as shown in Figure 7. It should be noted that the topological mapping of internodal CVs shows spatial correspondence with the connections of the prototypical networks (Figure 5). The result demonstrates that our clustering and reallocation procedures for classing synchrostates well keep the topological consistency of synchrostates separated into different clusters.

3.3 | Recurrent synchrostates underlying fundamental cognitive functions

According to the matrices of interstate transition probabilities, the digraphs of the Markov chain structures with all linked synchrostates were constructed for non-task idle state and reasoning process, respectively (Figure 8).

In the state transition process of the non-task period, all the types of synchrostates exhibit the characteristic of aperiodical recurrence, which represents the property of being accessible from all states that are accessible. Thus, the Markov chain can be represented by the set

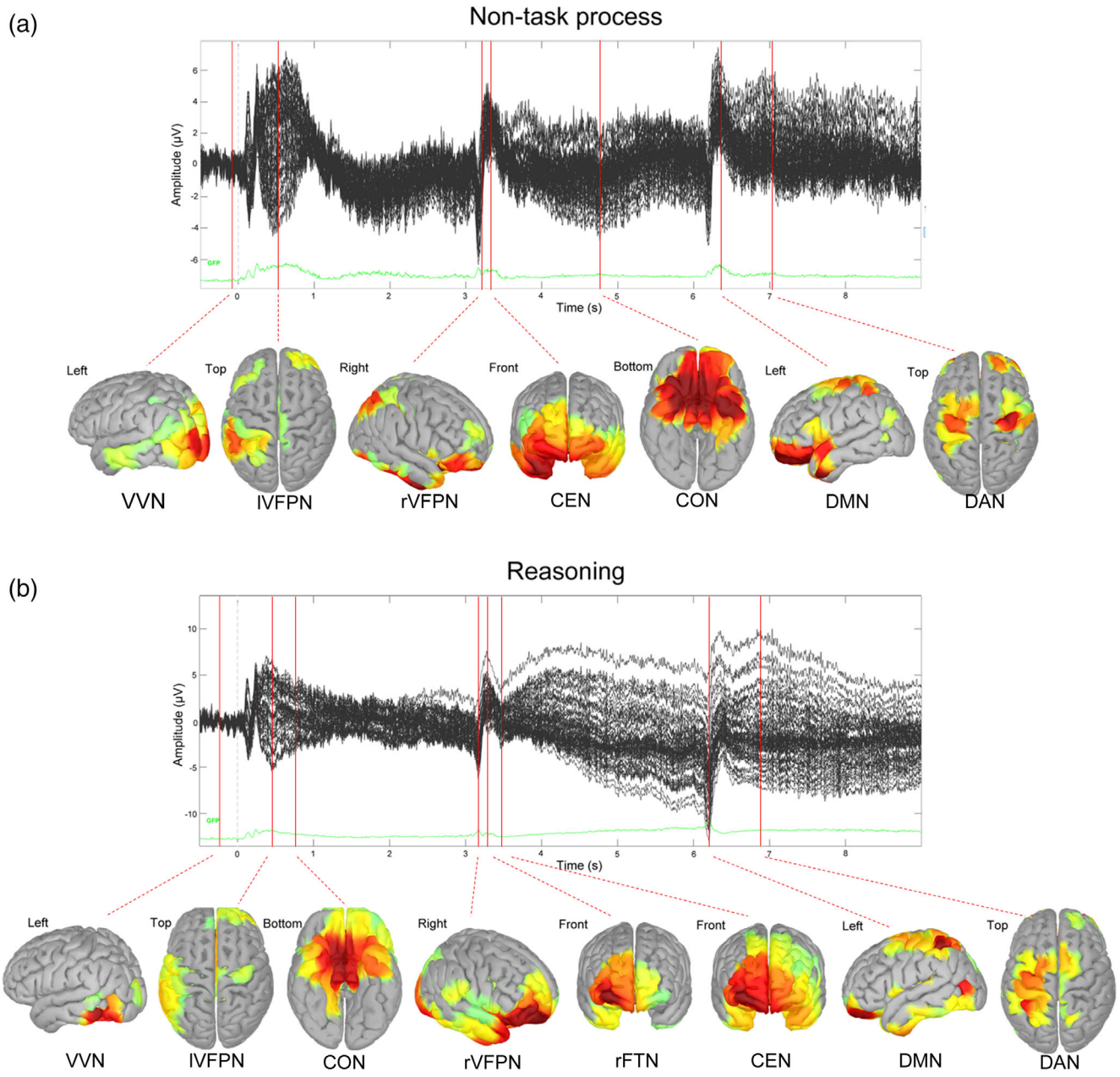

FIGURE 6 Sequential cortical current maps at major peaks and waveforms of grand average ERP during (a) non-task and (b) reasoning processes

of {DMN, CEN, DAN, CON, lVFPN, rVFPN, VVN}. The seven synchrostates have relatively even probabilities in occurrence during the non-task idle process (10.2–17.5%) (Figure 8a), in which the fractional occupancy of DMN, DAN, and VVN has achieved nearly half of the total time windows (16.4, 17.5, and 15.7%). In the reasoning process, the occurrence of different synchrostates has been moderately changed. The fractional occupancy of DMN, CON, lVFPN, and rVFPN is significantly dropped to 14.3% (ANOVA: p = .0010), 8.7% (ANOVA: p < .0001), 11.7% (ANOVA: p = .0237), and 12% (ANOVA: p = .0157), respectively (Figure 8c). Although there is no significant change in CEN and DAN from the non-task to the reasoning process, the interstate transitions occurring from other synchrostates toward CEN and DAN become more frequent (Figure 8c,d).

As the large-scale intrinsic networks in the human brain, DMN, CEN, DAN, VVN, and ventral attention system have been identified as fundamental to cognitive functions of the brain (Sridharan, Levitin, & Menon, 2008). Therefore, it is not surprising that the six networks aperiodically recur in both the non-task and reasoning processes. As a well-known functional network responding to high-level cognitive functions, CEN plays a crucial role in maintaining and using the information in working memory, problem solving, and decision making. DMN is sometimes referred to as the task-negative network, since the response in DMN usually proportionally and antagonistically relates with the demands of general external cognitive tasks. By contrast, as the task-positive network, DAN typically responds to activation increase to attention-demanding tasks (Calhoun & Adali, 2012;

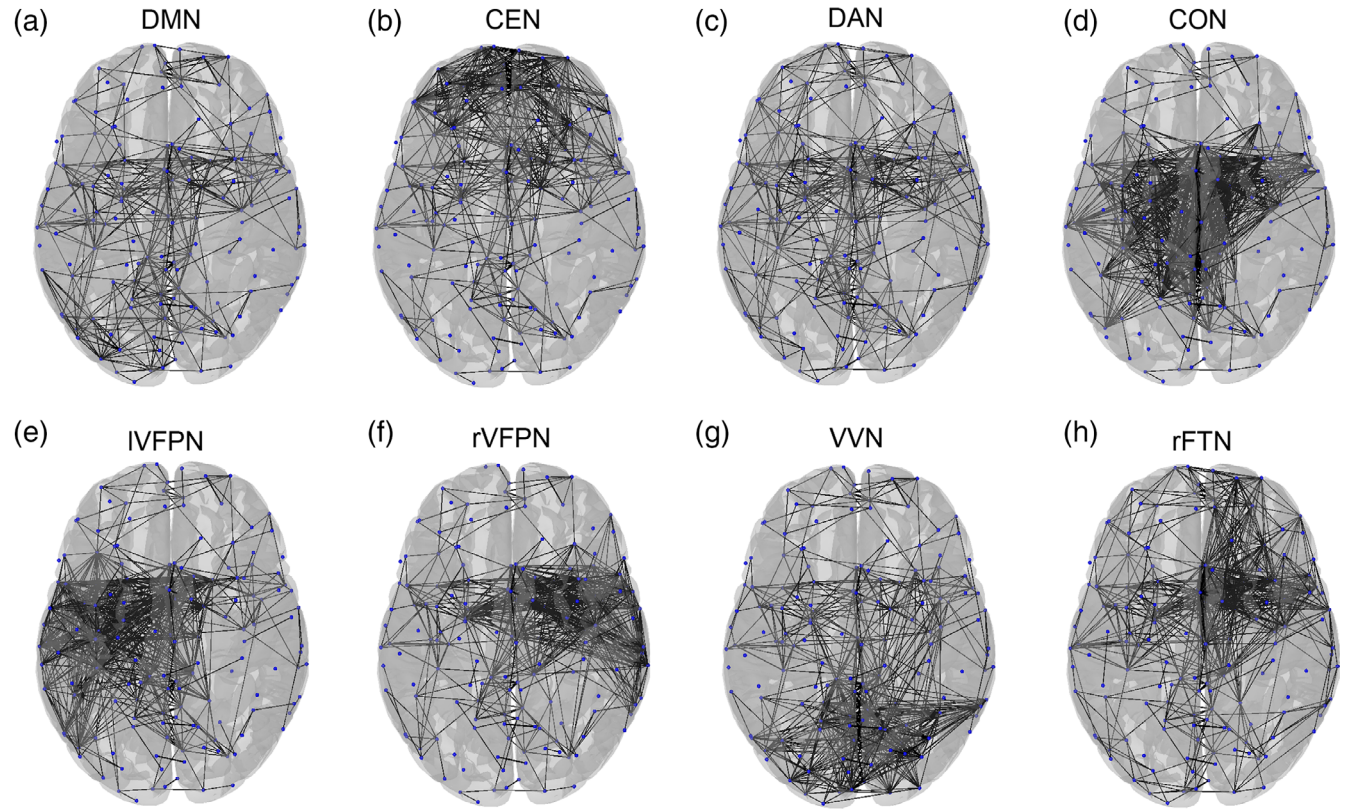

FIGURE 7 Topological mapping of internodal CVs from the synchrostates belonging to eight clusters. (a–h) refer to default mode network (DMN), central executive network (CEN), dorsal attention network (DAN), cingulo-opercular network (CON), left ventral frontoparietal network (lVFPN), right frontotemporal network (rVFPN), ventral visual network (VVN), and right frontotemporal network (rFTN), respectively. In each topological map, the lines represent internodal CVs less than 0.4

Menon, 2012). The opposite relationship in response activation can be observed in this study from the temporal measurements of synchrostates. The fractional occupancy of DMN is decreased from non-task idle state to the reasoning process, whereas increase can be found in the averaged occurrence of DAN (Figure 9a). On the other hand, DAN and ventral attention network constitute two sensory orienting systems in the human brain. While DAN mediates the top-down attentional control, the ventral frontoparietal network (VFPN) constitutes a bottom-up ventral attention system that might be involved in detecting unexpected stimuli and driving shifts of attention focus (Erel & Levy, 2016). It should be noticed that focused attention will inhibit the activity of VFPN to prevent reorienting to distracting events (Farrant & Uddin, 2015). From Figure 9a, we can find that the fractional occupancy of DAN is also opposite to those of lVFPN and rVFPN, manifested as the promotion in DAN but the inhibition in lVFPN and rVFPN from non-task to reasoning process. Besides, VVN is responsible for processing sensory input from multiple sensory modalities (Foley & Matlin, 2015), and it is usually described as the "what" stream related to object recognition and form representation. The connections in VVN are extended to the medial temporal lobe that stores long-term memory information (Schneider, 1969).

Specifically, the occurrence of CON is also dropped from non-task to the reasoning process, when CON becomes a transient state, as well as the reasoning-triggered rFTN with the lowest fractional occupancy (8%). Previous studies suggest that the functional role of CON is particularly difficult to characterize because of its pervasive activity and frequent co-activation with other control-related networks. It is likely that tonic alertness (i.e., sustained attention) is a fundamental function of CON, which refers to a sustained and endogenously maintained top-down controlling process (Coste & Kleinschmidt, 2016; Sadaghiani & D'Esposito, 2014; Vossel, Geng, & Fink, 2014).

In the non-task process of the brain, the recurrent synchrostates DMN, CEN, DAN, CON, lVFPN, rVFPN, and VVN exhibit interactively reachable transitions (Figure 8a), indicating the deterministic occurrence of these fundamental network topologies. While in the reasoning condition, the transient synchrostates, CON and rFTN, can also access the recurrent functional networks via rapid topological reorganization, clearly demonstrating the high predictability of the recruitment of DMN, CEN, DAN, lVFPN, rVFPN, and VVN, while being involved in the cognitive or non-task process (Figure 8a,c).

3.4 | Transient rFTN mediating imagination and creative thinking

The occurrence of rFTN is less than what the other recurrent functional networks occupy in the time domain (Figure 8c). Besides the

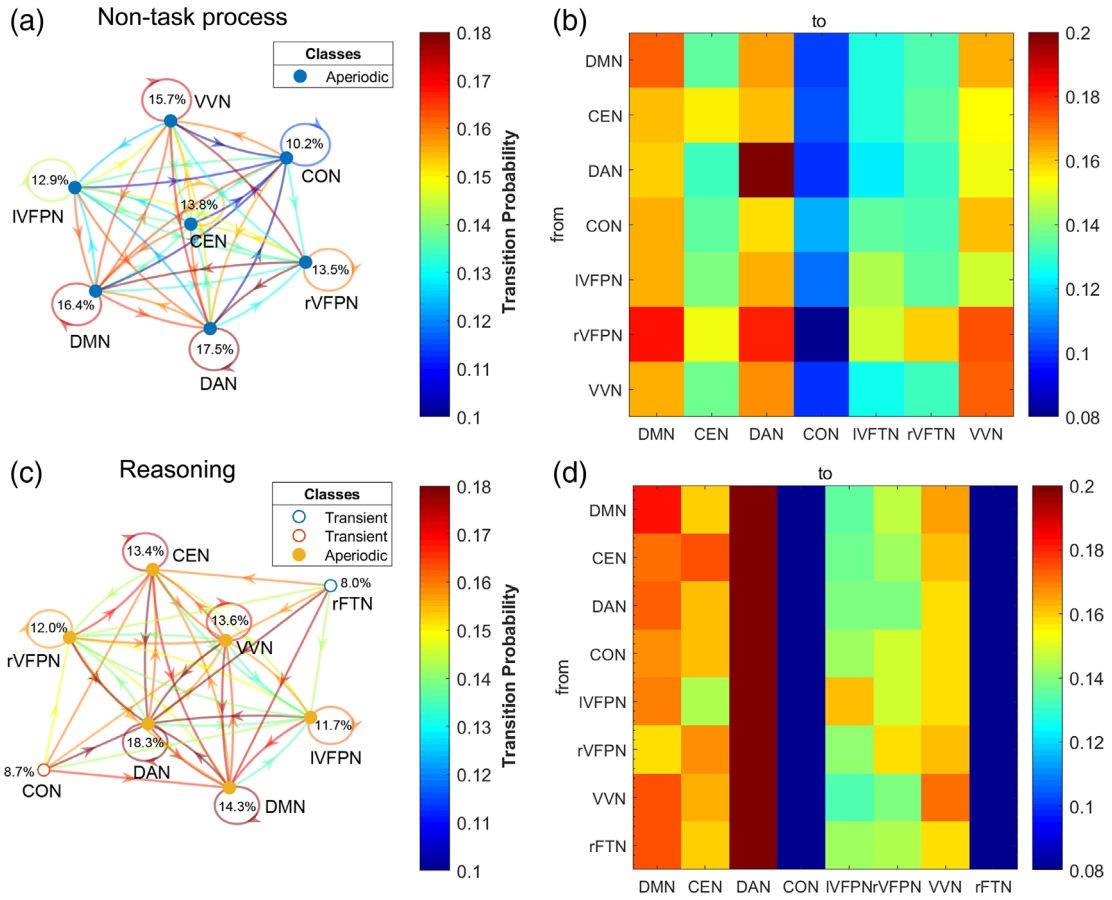

FIGURE 8 Digraphs and matrices of transition probabilities during (a, b) non-task idle state and (c, d) reasoning process. In the digraphs, each synchrostate in a Markov chain is marked as a node. The number beside each state refers to fractional occupancy, and directed edges indicate strong transitions with probabilities greater than .1. The colors of edges (a, c) and matrix elements (b, d) represent normalized transition probabilities (i.e., the sum of each row of p equals 1), with the values indicated in the corresponding color bars

low fractional occupancy, the network has been less likely reached by other states and there is little return from its accessing states. Therefore, it is identified as a "transient" class in the Markov chain. Baker et al. (2014) suggest that the occurrence of transient states might be a representation of temporal variability in the functional connectivity of brain network. In a Markov chain, transient states are usually unpredictable and eventually switch to recurrent states (Häggström, 2002).

It is noteworthy that rFTN only emerges in the reasoning process. Although taking up the lowest proportion in the total time windows, rFTN has special significance for high-level logical thinking activity. While engaging in cognitive processing, the frontal lobes can be seen as responsible for idea generation, and the temporal lobes play an important role in idea editing and evaluation (Flaherty, 2005). There is a common opinion that the right hemisphere is dominant for geometric and visuospatial analysis and is also highly involved in mathematical reasoning and creativity (Joseph, 1988). In a longitudinal functional magnetic resonance imaging study, alteration of rFTN clusters including the right DLPFC and temporal areas has been found to predict enhanced creative ability of the brain, especially in longitudinal gains (Chen et al., 2016). These pieces of evidence suggest that the sporadic recruitment of rFTN in the reasoning process might be responsive for high-order thinking activity.

3.5 | Specific Markov process of synchrostate transitions in the math-gifted brain

In the statistical analysis of the temporal measurements in synchrostate transitions, there is no significant between-conditions difference in CEN (Figure 9). However, the between-groups comparisons reveal differential Markov process of mental activities responding to non-task or logical reasoning, involving synchrostate transition mode general to high intelligence or specific to the talent in mathematics.

3.5.1 | Temporal superiority in maintaining CEN and rFTN topologies

Within 180 time windows of a cognitive process, the allocation of brain network resources for the dominance of DMN, CEN, VVN, and rFTN is significantly different between math-gifted and control groups in terms of fractional occupancy and mean duration (Figure 9).

Compared to the average-ability control subjects, the math-gifted adolescents had less occurrence and shorter duration of DMN during non-task (ANOVA: p = .0025 for fractional occupancy; p < .0001 for mean duration) and reasoning process (ANOVA: p < .0001 for

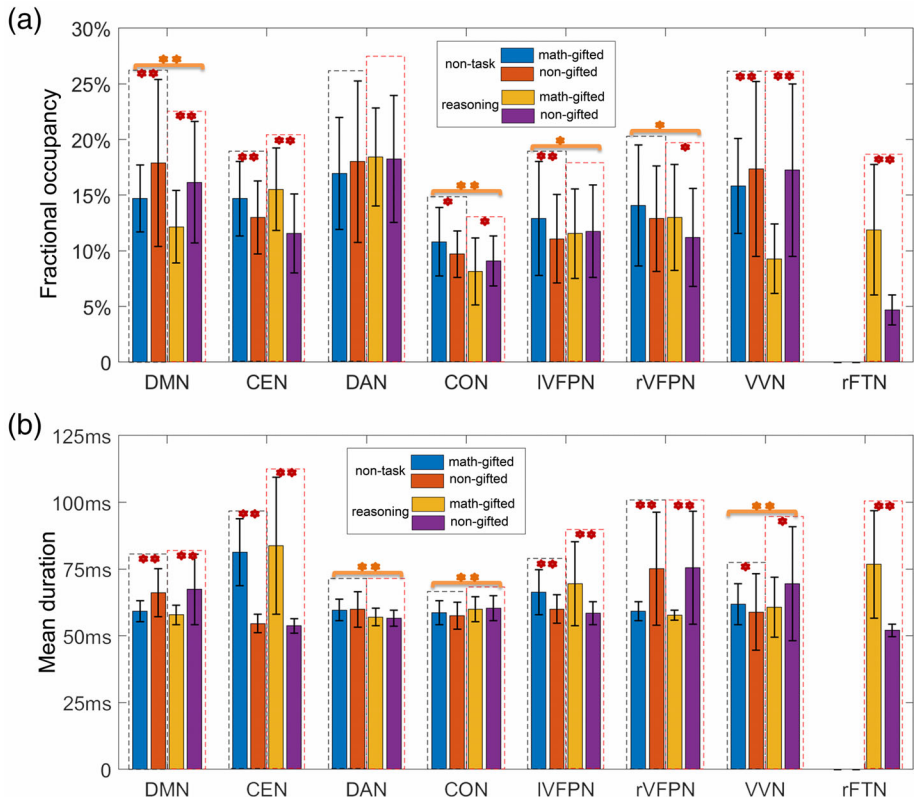

FIGURE 9 Statistical bars of (a) fractional occupancy and (b) mean duration in eight classes of synchrostates, for comparisons between task conditions and between groups [** indicates significance level $p < .01$ in the analysis of variance (ANOVA) and *$p < .05$]

fractional occupancy; $p < .0001$ for mean duration). As the task-negative network, DMN is commonly activated in unfocused activity on the outside world when the brain is at wakeful rest, but it is usually deactivated in goal-oriented tasks (Anticevic et al., 2012; Broyd et al., 2009). The less temporal occurrence and duration of DMN in the math-gifted brain means more task-relevant network topologies have been organized in the limited time frame of cognitive processes.

Conversely, the math-gifted adolescents show more frequent recruitment and longer duration of CEN in both the processes, as compared to non-gifted subjects (ANOVA: $p = .0048$ for fractional occupancy and $p < .0001$ for the mean duration in non-task condition; ANOVA: $p < .0001$ for fractional occupancy and $p < .0001$ for the mean duration in reasoning condition). Previous studies have consistently demonstrated higher-level cognitive control and executive attention of the math-gifted brain (Desco et al., 2011; Zhang et al., 2015). In line with the conclusion, the math-gifted adolescents outnumbered the controls in the baseline-to-reasoning increase (Figure 9a), strongly suggesting more active recruitment of the central executive controlling system in the reasoning process. Moreover, the superior executive functions of the math-gifted adolescents involved in reasoning were reflected by the behavioral data, in which they achieved higher mean response accuracy and significantly shorter reaction time for accomplishing the reasoning task than the average-level control subjects. Besides, there is a covariation tendency in the feature distribution between the subject's response accuracy and fractional occupancy/mean duration of CEN (Figure 10).

The math-gifted group also outperformed the non-gifted subjects in recruiting rFTN during the reasoning process, with higher fractional occupancy (ANOVA: $p < .0001$) and longer mean duration (ANOVA: $p < .0001$) (Figure 9). This finding coincides with previous neuroimaging studies, which have demonstrated that math-gifted adolescents have a higher reliance on the right-lateral cognitive functions, primarily involving the frontal and temporal lobes, part of the parietal lobe, and the postcentral gyrus and premotor cortex (Desco et al., 2011; Prescott et al., 2010). From integrated empirical evidence, the well-developed cognitive controlling functions of the anterior neural system including the PFC, frontal lobe, and the AC are usually viewed as the neural feature common to high-level general intelligence, an essential component of mathematical giftedness (Zhang et al., 2017). In the current study, more frequent recruitment and relatively stable topology of rFTN might be more specific to the talent in mathematics, because the cognitive functions in the right-lateral frontal lobe can be particularly connected to gifted thinking abilities in mathematics, including spatial information processing, reasoning, and creative thinking (Prescott et al., 2010).

3.5.2 | Robust self-loops of CEN and rFTN in state transitions during reasoning

The temporally stable CEN and rFTN in the math-gifted brain are manifested as a higher probability in their self-transitions, particularly in the Markov chain constructed from the reasoning process (Bootstrapped ANOVAs with FDR correction: $p < .05$) (Figure 11b).

In a Markov chain, a self-loop representing the transition from one state back to itself ensures its aperiodicity and forms the basis of

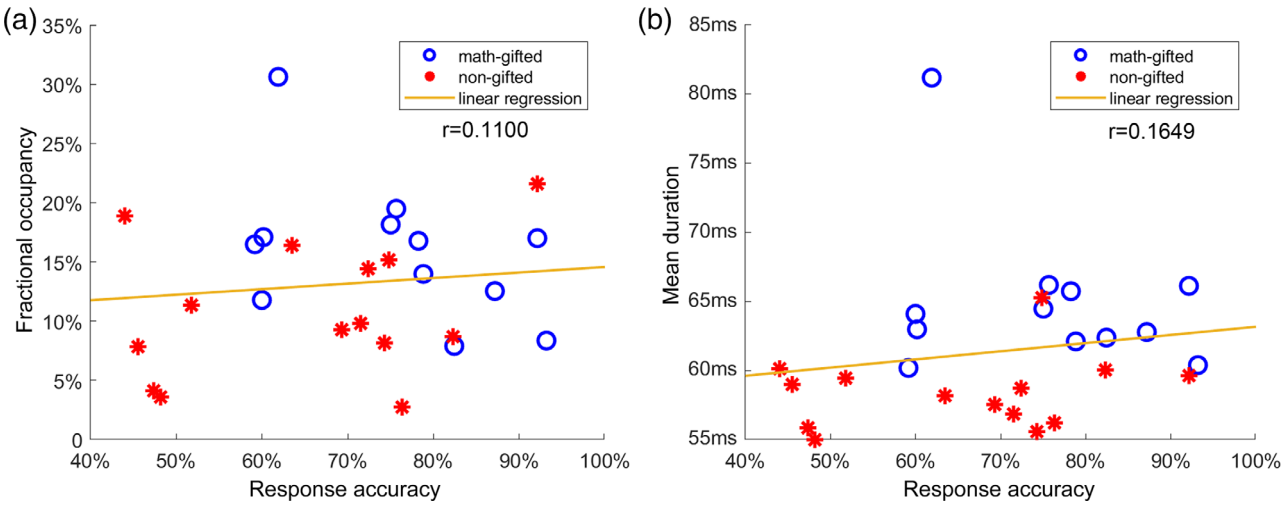

FIGURE 10 Feature distribution and linear regression (a) between the subject's response accuracy and fractional occupancy, and (b) between response accuracy and mean duration of central executive network (CEN). *r* refers to the correlation coefficient between two variables

"lazy" chain (Häggström, 2002), which can be ascribed to the state inertia, durability or persistence. From the perspective of brain network dynamics, a self-loop state indicates the temporal duration of a network structure being maintained over a sub-second time scale. Denser self-transitions of CEN in the math-gifted brain are especially important for goal-oriented persistence and high task commitment (Navas-Sánchez et al., 2016), by maintaining ongoing information processing for tasks that require focused efforts and attention toward achieving the final goal. The result keeps good consistency with the previous finding that math-gifted adolescents can recruit an enhanced task-related global neuronal workspace with strengthened synchronization activity at anterior cortices vertices of the frontoparietal network, by virtue of more effortful cognitive processing (Zhang et al., 2015). With regard to rFTN, more self-loops in the math-gifted brain mean high probability in staying at itself, which is beneficial for information transfer and storage through durational information communication of the transient network pattern.

3.5.3 | Adaptive network reconfiguration toward CEN and rFTN topologies

The increased transitions from other synchrostates toward CEN and rFTN in the Markov chain also correlate with more frequent recruitment of the two connectivity patterns in the math-gifted brain. The parieto-frontal integration theory suggests the crucial role of coordination of multiple brain regions and information communication among association cortices in logical reasoning (Jung & Haier, 2007). Moreover, cognitive functions depend on the adaptive self-organization of large-scale neuronal assemblies, that is, rapid redistribution of spatial connections in a functional network (Bassett et al., 2006; Kitzbichler et al., 2009). During the reasoning task of this study, the functional brain networks of the math-gifted adolescents show significantly promoted probabilities in reconfiguring to CEN from DMN, DAN, CON, lVFPN, rVFPN, and rFTN. Additionally, there are also higher probabilities in switching to rFTN from the other seven synchrostates in the math-gifted group (Figure 11b). The results indicate higher predictability and certainty of CEN and rFTN organized during the reasoning process in the math-gifted brain. For the math-gifted adolescents, the specific Markov process of synchrostate transitions, that is, the different route of functional network reconfigurations, indicates greater capacity in driving reorganization of the large-scale cortical network to better adapt to central executive controlling function and high-order thinking activity involved in reasoning.

3.6 | Main limitations

There still may be limitations with respect to the generality of the methods and findings. The first problem is the single-trial EEG analysis. Conventional microstate functional connectivity is based on grand average multiple-subject ERP to get stable EEG microstates (ERP components). Although single-trial analysis takes account of trial-to-trial variation in brain activities and provides enough samples in statistical comparisons, it is inevitable to result in low signal to noise ratio. Second, the determination of prototypical network topologies is crucial to label synchrostates and construct Markov chains. In this study, we used iterative similarity tests to repeatedly update the prototypes. The stopping criterion is whether the topological similarity of node centrality of intra-cluster synchrostates can be significantly improved in statistical tests after a reallocation. The standard can make sure that the total data distribution achieves an optimal consistency in separating synchrostates, but a single cluster may be unable to get the best intra-cluster consistency. Besides, the AHC clustering procedure requires the setting of the number of initial clusters, which depends on the prior knowledge for fundamental large-scale cortical networks and neurocognitive subnetworks. Data-driven clustering method for

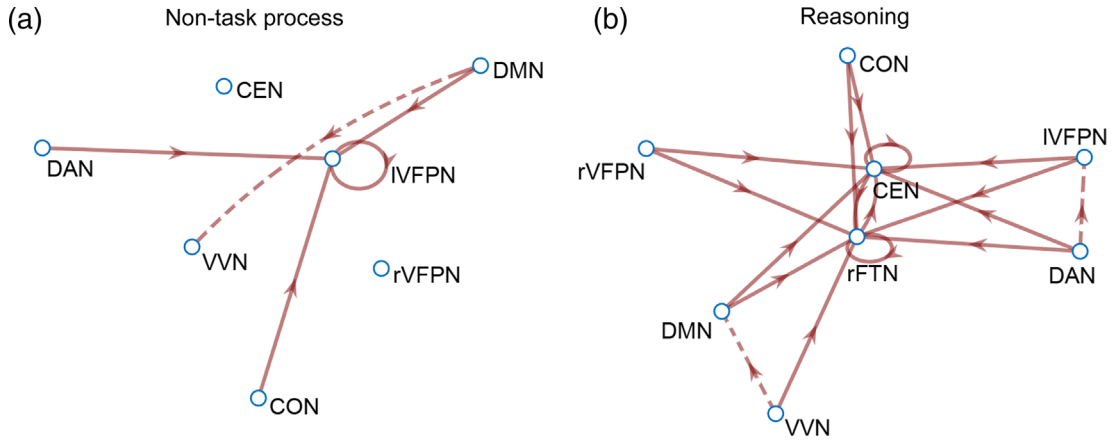

FIGURE 11 Between-groups differences in interstate transition probabilities of the Markov chains during (a) non-task idle state and (b) reasoning process. Compared to the non-gifted control group, the dotted lines refer to significant lower transition probabilities for the math-gifted group and the solid lines higher probabilities [Bootstrapped analysis of variance (ANOVA) with false discovery rate (FDR) correction: $p < .05$]

synchrostates without a prior specification of either cluster number or network form is worthy to be systematically explored, such as orthogonal minimal spanning tree (Dimitriadis, Salis, Tarnanas, & Linden, 2017). Third, in source trace analysis, we used the MNE to solve the inverse problem and the sLORETA as the normalization method of current density mapping. Other classical source transformation methods, such as linearly constrained minimum variance beamformer, dipole modeling, or other surrogate analysis method, should be further tested to cross-validate the reliability of source-space synchrostate analysis.

4 | CONCLUSION

For the math-gifted adolescents who are of particular concern in the field of educational neuroscience, it is the first time that transition dynamics among a limited number of functional neurocognitive networks is investigated and the temporal features are extracted for detecting differences in the brain dynamics related to cognitive ability levels of advanced mathematical thinking. Instead of usual EEG scalp potential microstates, large-scale brain networks of cortical sources are treated as quasi-stable brain states to construct Markov chains of interstate transitions.

By discretizing phase-lock patterns of ongoing brain activity, our study has observed episodic and heterogeneous synchrostates fluctuating at the millisecond time scale. The time-sequential synchrostates contribute to the construction of probabilistic transition models of the global neuronal networks in both condition- and subject-centered manner. Neural correlations with mathematical giftedness can be reflected in the interstate transition patterns during the reasoning process. The math-gifted adolescents show higher fractional occupancy and mean duration in maintaining CEN and rFTN connectivity patterns, as well as greater transition capacity both in their self-loops and from other synchrostates, than their average-ability peers. In the Markov process of switching functional connectivity states of the brain network, frequent recurrence of CEN is beneficial for maintaining attention for task goal, effectively using the information in working memory and making a correct decision. More occurrence of transient rFTN promotes the predictability of implementing high-order spatial processing, imagine and creative thinking.

The Markov chain modeling of synchrostate transition provides new evidence and extends our knowledge about math-gifted brain that enhanced functional connectivity in the frontoparietal network is underpinned by temporally more stable network topology and higher reorganization capacity from other connectivity patterns. The specific transition dynamics of connectivity patterns in the frontoparietal network facilitate central executive controlling function and high-order thinking activity of the math-gifted adolescents while handling the long-chain deductive reasoning.

ACKNOWLEDGMENTS

This work was supported in part by the Natural Science Foundation of China under Grants 31600862, 61773114, and 31900710; the Support Program of Excellent Young Talents in Universities of Anhui Province under Grant gxyqZD2017064; the China Scholarship Council Fund under Grant 201808340011; the Scientific Research Innovation Project of Bengbu Medical College under Grant BYKC201905; the Fundamental Research Funds for the Central Universities under Grant CDLS-2018-04; and Key Laboratory of Child Development and Learning Science (Southeast University), Ministry of Education.

CONFLICT OF INTEREST

The authors declare no potential conflict of interest.

DATA AVAILABILITY STATEMENT

The data used to support the findings of this study are available from the corresponding author upon reasonable request.

ORCID

Li Zhang https://orcid.org/0000-0001-9473-7799

Jing Wang https://orcid.org/0000-0002-3286-073X

Haixian Wang https://orcid.org/0000-0001-8220-9737

REFERENCES

Allen, E. A., Damaraju, E., Plis, S. M., Erhardt, E. B., Eichele, T., & Calhoun, V. D. (2014). Tracking whole-brain connectivity dynamics in the resting state. *Cerebral Cortex*, *24*(3), 663–676.

Anticevic, A., Cole, M. W., Murray, J. D., Corlett, P. R., Wang, X. J., & Krystal, J. H. (2012). The role of default network deactivation in cognition and disease. *Trends in Cognitive Sciences*, *16*(12), 584–592.

Baker, A. P., Brookes, M. J., Rezek, I. A., Smith, S. M., Behrens, T., Probert Smith, P. J., & Woolrich, M. (2014). Fast transient networks in spontaneous human brain activity. *eLife*, *3*(3), e01867.

Banfield, T. (2005). Ability grouping for mathematically gifted adolescent boys. *International Education Journal*, *6*(2), 141–149.

Bassett, D. S., Meyer-Lindenberg, A., Achard, S., Duke, T., & Bullmore, E. (2006). Adaptive reconfiguration of fractal small-world human brain functional networks. *Proceedings of the National Academy of Sciences*, *103*(51), 19518–19523.

Bassett, D. S., Wymbs, N. F., Porter, M. A., Mucha, P. J., Carlson, J. M., & Grafton, S. T. (2011). Dynamic reconfiguration of human brain networks during learning. *Proceedings of the National Academy of Sciences*, *108*(18), 7641–7646.

Bola, M., & Sabel, B. A. (2015). Dynamic reorganization of brain functional networks during cognition. *NeuroImage*, *114*, 398–413.

Bressler, S. L., & Menon, V. (2010). Large-scale brain networks in cognition: Emerging methods and principles. *Trends in Cognitive Sciences*, *14*(6), 277–290.

Broyd, S. J., Demanuele, C., Debener, S., Helps, S. K., James, C. J., & Sonuga-Barke, E. J. (2009). Default-mode brain dysfunction in mental disorders: A systematic review. *Neuroscience & Biobehavioral Reviews*, *33*(3), 279–296.

Bullmore, E., & Sporns, O. (2009). Complex brain networks: Graph theoretical analysis of structural and functional systems. *Nature Reviews Neuroscience*, *10*(3), 186–198.

Calhoun, V. D., & Adali, T. (2012). Multisubject independent component analysis of fMRI: A decade of intrinsic networks, default mode, and neurodiagnostic discovery. *IEEE Reviews in Biomedical Engineering*, *5*, 60–73.

Chen, Q., Beaty, R. E., Wei, D., Yang, J., Sun, J., Liu, W., … Qiu, J. (2016). Longitudinal alterations of frontoparietal and frontotemporal networks predict future creative cognitive ability. *Cerebral Cortex*, *28*(1), 103–115.

Coste, C. P., & Kleinschmidt, A. (2016). Cingulo-opercular network activity maintains alertness. *NeuroImage*, *128*, 264–272.

Daly, I., Sweeney-Reed, C. M., & Nasuto, S. J. (2013). Testing for significance of phase synchronisation dynamics in the EEG. *Journal of Computational Neuroscience*, *34*(3), 411–432.

Delorme, A., & Makeig, S. (2004). EEGLAB: An open source toolbox for analysis of single-trial EEG dynamics including independent component analysis. *Journal of Neuroscience Methods*, *134*(1), 9–21.

Desco, M., Navas-Sanchez, F. J., Sanchez-González, J., Reig, S., Robles, O., Franco, C., … Arango, C. (2011). Mathematically gifted adolescents use more extensive and more bilateral areas of the fronto-parietal network than controls during executive functioning and fluid reasoning tasks. *NeuroImage*, *57*(1), 281–292.

Dimitriadis, S. I., Laskaris, N. A., & Micheloyannis, S. (2015). Transition dynamics of EEG-based network microstates during mental arithmetic and resting wakefulness reflects task-related modulations and developmental changes. *Cognitive Neurodynamics*, *9*(4), 371–387.

Dimitriadis, S. I., Laskaris, N. A., & Tzelepi, A. (2013). On the quantization of time-varying phase synchrony patterns into distinct functional connectivity microstates (FCμstates) in a multi-trial visual ERP paradigm. *Brain Topography*, *26*(3), 397–409.

Dimitriadis, S. I., López, M. E., Maestu, F., Pereda, E., , & (2019). Modeling the switching behavior of functional connectivity microstates (FCμstates) as a novel biomarker for mild cognitive impairment. *Frontiers in Neuroscience*, *13*, 542

Dimitriadis, S. I., Salis, C., Tarnanas, I., & Linden, D. E. (2017). Topological filtering of dynamic functional brain networks unfolds informative chronnectomics: A novel data-driven thresholding scheme based on orthogonal minimal spanning trees (OMSTs). *Frontiers in Neuroinformatics*, *11*, 28.

Doesburg, S. M., Roggeveen, A. B., Kitajo, K., & Ward, L. M. (2008). Large-scale gamma-band phase synchronization and selective attention. *Cerebral Cortex*, *18*(2), 386–396.

Duc, N. T., & Lee, B. (2019). Microstate functional connectivity in EEG cognitive tasks revealed by a multivariate Gaussian hidden Markov model with phase locking value. *Journal of Neural Engineering*, *16*(2), 026033.

Duncan, J. (2013). The structure of cognition: Attentional episodes in mind and brain. *Neuron*, *80*(1), 35–50.

Erdős, P., & Rényi, A. (1961). On the strength of connectedness of a random graph. *Acta Mathematica Academiae Scientiarum Hungarica*, *12*(1–2), 261–267.

Erel, H., & Levy, D. A. (2016). Orienting of visual attention in aging. *Neuroscience and Biobehavioral Reviews*, *69*, 357–380.

Farrant, K., & Uddin, L. Q. (2015). Asymmetric development of dorsal and ventral attention networks in the human brain. *Developmental Cognitive Neuroscience*, *12*, 165–174.

Flaherty, A. W. (2005). Frontotemporal and dopaminergic control of idea generation and creative drive. *The Journal of Comparative Neurology*, *493*(1), 147–153.

Foley, H., & Matlin, M. (2015). *Sensation and perception*, London: Psychology Press.

Fries, P. (2005). A mechanism for cognitive dynamics: Neuronal communication through neuronal coherence. *Trends in Cognitive Sciences*, *9*(10), 474–480.

Gagniuc, P. A. (2017 & *Markov chains: From theory to implementation and experimentation*, Hoboken, NJ: John Wiley & Sons.

Gärtner, M., Brodbeck, V., Laufs, H., & Schneider, G. (2015). A stochastic model for EEG microstate sequence analysis. *NeuroImage*, *104*, 199–208.

Goel, V., & Dolan, R. J. (2001). Functional neuroanatomy of three-term relational reasoning. *Neuropsychologia*, *39*(9), 901–909.

Gramfort, A., Papadopoulo, T., Olivi, E., & Clerc, M. (2010). OpenMEEG: Opensource software for quasistatic bioelectromagnetics. *Biomedical Engineering Online*, *9*(1), 45.

Häggström, O. (2002). *Finite Markov chains and algorithmic applications*, Cambridge: Cambridge University Press.

Herrmann, C. S., Fründ, I., & Lenz, D. (2010). Human gamma-band activity: A review on cognitive and behavioral correlates and network models. *Neuroscience and Biobehavioral Reviews*, *34*(7), 981–992.

Howard, M. W., Rizzu To, D. S., Caplan, J. B., Madsen, J. R., Lisman, J., Aschenbrenner-Scheibe, R., … Kahana, M. J. (2003). Gamma oscillations correlate with working memory load in humans. *Cerebral Cortex*, *13*(12), 1369–1374.

Jamal, W., Das, S., & Maharatna, K. (2013). *Existence of millisecond-order stable states in time-varying phase synchronization measure in EEG signals*. The 35th Annual International Conference of the IEEE Engineering in Medicine and Biology Society (EMBC), pp. 2539–2542.

Jamal, W., Das, S., Maharatna, K., Apicella, F., Chronaki, G., Sicca, F., … Muratori, F. (2015). On the existence of synchrostates in multichannel EEG signals during face-perception tasks. *Biomedical Physics & Engineering Express*, *1*(1), 015002.

Jamal, W., Das, S., Oprescu, I. A., & Maharatna, K. (2014). Prediction of synchrostate transitions in EEG signals using Markov chain models. *IEEE Signal Processing Letters*, *22*(2), 149–152.

Jarvis, J. P., & Shier, D. R. (1999). Graph-theoretic analysis of finite Markov chains. In *Applied Mathematical Modeling: A Multidisciplinary Approach* (p. 85). Boca Raton, Florida: CRC Press.

Joseph, R. (1988). The right cerebral hemisphere: Emotion, music, visual-spatial skills, body-image, dreams, and awareness. *Journal of Clinical Psychology*, *44*(5), 630–673.

Jung, R. E., & Haier, R. J. (2007). The parieto-frontal integration theory (P-FIT) of intelligence: Converging neuroimaging evidence. *Behavioral & Brain Sciences*, *30*, 135–154.

Karamzadeh, N., Medvedev, A., Azari, A., Gandjbakhche, A., & Najafizadeh, L. (2013). Capturing dynamic patterns of task-based functional connectivity with EEG. *NeuroImage*, *66*, 311–317.

Kitzbichler, M. G., Smith, M. L., Christensen, S. R., & Bullmore, E. (2009). Broadband criticality of human brain network synchronization. *PLoS Computational Biology*, *5*(3), e1000314.

Lachaux, J. P., Rodriguez, E., Martinerie, J., & Varela, F. J. (1999). Measuring phase synchrony in brain signals. *Human Brain Mapping*, *8*(4), 194–208.

Langer, N., Pedroni, A., Gianotti, L. R., Hänggi, J., Knoch, D., & Jäncke, L. (2012). Functional brain network efficiency predicts intelligence. *Human Brain Mapping*, *33*(6), 1393–1406.

Mahyari, A. G., Zoltowski, D. M., Bernat, E. M., & Aviyente, S. (2016). A tensor decomposition-based approach for detecting dynamic network states from EEG. *IEEE Transactions on Biomedical Engineering*, *64*(1), 225–237.

Menon, V. (2012). Functional connectivity, neurocognitive networks, and brain dynamics. In M. I. Rabinovich, K. J. Friston, & P. Varona (Eds.), *Principles of brain dynamics: Global state interactions* (pp. 27–47). Cambridge, MA: MIT Press.

Michel, C. M., & Koenig, T. (2017). EEG microstates as a tool for studying the temporal dynamics of whole-brain neuronal networks: A review. *NeuroImage*, *108*, 577–593.

Myers, T., Carey, E., & Szűcs, D. (2017). Cognitive and neural correlates of mathematical giftedness in adults and children: A review. *Frontiers in Psychology*, *8*, 1646.

Navas-Sánchez, F. J., Aleman-Gomez, Y., Sanchez-Gonzalez, J., Guzman-De-Villoria, J. A., Franco, C., Robles, O., … Desco, M. (2014). White matter microstructure correlates of mathematical giftedness and intelligence quotient. *Human Brain Mapping*, *35*(6), 2619–2631.

Navas-Sánchez, F. J., Carmona, S., Alemán-Gómez, Y., Sánchez-González, J., Guzmán-de-Villoria, J., Franco, C., … Desco, M. (2016). Cortical morphometry in frontoparietal and default mode networks in math-gifted adolescents. *Human Brain Mapping*, *37*(5), 1893–1902.

Prescott, J., Gavrilescu, M., Cunnington, R., O'Boyle, M. W., & Egan, G. F. (2010). Enhanced brain connectivity in math-gifted adolescents: An fMRI study using mental rotation. *Cognitive Neuroscience*, *1*(4), 277–288.

Rothmaler, K., & Ivanova, G. (2018). The HEURECA method: Tracking multiple phase coupling dynamics on a single trial basis. *Journal of Neuroscience Methods*, *307*, 138–148.

Rukat, T., Baker, A., Quinn, A., & Woolrich, M. (2016). Resting state brain networks from EEG: hidden Markov states vs. classical microstates, preprint arXiv: 1606.02344.

Sadaghiani, S., & D'Esposito, M. (2014). Functional characterization of the cingulo-opercular network in the maintenance of tonic alertness. *Cerebral Cortex*, *25*(9), 2763–2773.

Sakkalis, V. (2011). Review of advanced techniques for the estimation of brain connectivity measured with EEG/MEG. *Computers in Biology and Medicine*, *41*(12), 1110–1117.

Schmidt, B. T., Ghuman, A. S., & Huppert, T. J. (2014). Whole brain functional connectivity using phase locking measures of resting state magnetoencephalography. *Frontiers in Neuroscience*, *8*, 141.

Schneider, G. E. (1969). Two visual systems. *Science*, *163*(3870), 895–902.

Solé-Casals, J., Serra-Grabulosa, J. M., Romero-Garcia, R., Vilaseca, G., Adan, A., Vilaró, N., & Bullmore, E. T. (2019). Structural brain network of gifted children has a more integrated and versatile topology. *Brain Structure and Function*, *224*(7), 2373–2383.

Sporns, O., Honey, C. J., & Kötter, R. (2007). Identification and classification of hubs in brain networks. *PLoS One*, *2*(10), e1049.

Sridharan, D., Levitin, D. J., & Menon, V. (2008). A critical role for the right fronto-insular cortex in switching between central-executive and default-mode networks. *Proceedings of the National Academy of Sciences*, *105*(34), 12569–12574.

Tadel, F., Baillet, S., Mosher, J. C., Pantazis, D., & Leahy, R. M. (2011). Brainstorm: A user-friendly application for MEG/EEG analysis. *Computational Intelligence and Neuroscience*, *2011*, 8.

van de Ville, D., Britz, J., & Michel, C. M. (2010). EEG microstate sequences in healthy humans at rest reveal scale-free dynamics. *Proceedings of the National Academy of Sciences*, *107*(42), 18179–18184.

van den Heuvel, M. P., & Sporns, O. (2013). Network hubs in the human brain. *Trends in Cognitive Sciences*, *17*(12), 683–696.

Vinck, M., Oostenveld, R., Wingerden, M. V., Battaglia, F., & Pennartz, C. M. A. (2011). An improved index of phase-synchronization for electrophysiological data in the presence of volume-conduction, noise and sample-size bias. *NeuroImage*, *55*(4), 1548–1565.

Vossel, S., Geng, J. J., & Fink, G. R. (2014). Dorsal and ventral attention systems: Distinct neural circuits but collaborative roles. *The Neuroscientist*, *20*(2), 150–159.

Winner, E. (2000). The origins and ends of giftedness. *American Psychologist*, *55*(1), 159–169.

Yule, P. G., Fox, J., Glasspool, D. W., & Cooper, R. P. (2013). *Modelling high-level cognitive processes*, London: Psychology Press.

Zhang, L., Gan, J. Q., & Wang, H. (2014). Optimized gamma synchronization enhances functional binding of fronto-parietal cortices in mathematically gifted adolescents during deductive reasoning. *Frontiers in Human Neuroscience*, *8*, 430.

Zhang, L., Gan, J. Q., & Wang, H. (2015). Mathematically gifted adolescents mobilize enhanced workspace configuration of theta cortical network during deductive reasoning. *Neuroscience*, *289*, 334–348.

Zhang, L., Gan, J. Q., & Wang, H. (2017). Neurocognitive mechanisms of mathematical giftedness: A literature review. *Applied Neuropsychology: Child*, *6*(1), 79–94.

SUPPORTING INFORMATION

Additional supporting information may be found online in the Supporting Information section at the end of this article.

How to cite this article: Zhang L, Gan JQ, Zhu Y, Wang J, Wang H. EEG source-space synchrostate transitions and Markov modeling in the math-gifted brain during a long-chain reasoning task. *Hum Brain Mapp*. 2020;41:3620–3636. https://doi.org/10.1002/hbm.25035